Journal of the Brazilian Society of Mechanical Sciences and Engineering (2024) 46:98
https://doi.org/10.1007/s40430-023-04627-7

TECHNICAL PAPER

Influence of approximation methods on the design of the novel low-order fractionalized PID controller for aircraft system

A. Idir[1,2] · **Y. Bensafia**[3] · **L. Canale**[4]

Received: 22 October 2022 / Accepted: 5 December 2023

Abstract
In this paper, the effect of approximation approaches on a novel low-order fractionalized proportional–integral–derivative (LOA/FPID) optimal controller based on the Harris Hawks optimization algorithm (HHOA) for airplane pitch angle control is studied. The Carlson, Oustaloup and Matsuda methods are used separately to approximate the fractional integral order of the fractionalized PID controller. This technique consists in introducing fractional-order integrators into the classical feedback control loop without modifying the overall equivalent closed loop transfer function. To validate the effectiveness of the suggested approach, performance indices, as well as transient and frequency responses, were used. The comparative study was performed, and the results show that the proposed reduced fractionalized PID based on HHO algorithm with Carlson controller is better in terms of percentage overshoot, settling time and rise time than other controllers.

Keywords Fractional calculus · Fractionalized order controllers · Integer order controllers · Aircraft system · Pitch angle · Approximation methods

1 Introduction

Fractional-order (FO) differential calculus, or fractional calculus, is an area of mathematics concerned with the expansion of well-known differentiation and integration operations to arbitrary orders. Thanks to correspondence between two mathematicians, Leibniz and L'Hospital [1], science began to deal with the field about 1695.

Fractional PID controllers offer advantages over traditional PID controllers in specific applications owing to their capability to introduce fractional-order derivatives and integrals [2]. These fractional-order components provide increased flexibility in capturing the dynamics of nonlinear systems, thereby enhancing control performance. The introduction of a memory effect through fractional-order components allows the controller to consider not only the current error but also historical error values, improving adaptability to changing system conditions [3]. Additionally, fractional derivatives and integrals enable a smoother transition between differentiation and integration, proving beneficial in systems with abrupt changes or varying dynamics. In certain cases, fractional-order controllers can enhance stability margins and robustness, particularly in systems characterized by long time delays. The extra degrees of freedom in fractional PID controllers can be tuned to reduce overshoot and settling time, resulting in an improved transient response [4].

Fractional-order PID has advanced rapidly over the past decades and has a wide range of applications in control engineering and research [5–9]. Pdlubny was the first to implement FOPID in 1997 [6]. Compared with the traditional PID tuning methods, Luo et al. [7] designed FOPID and FOPI controllers, which improved the system robustness and control performance. Bensafia et al. [8] used a fractionalized PID controller strategy to reduce effect noise in the conventional feedback control loop PID controller by introducing fractional-order filters. Idir et al. [9] have demonstrated the

Technical Editor: Flávio Silvestre.

✉ A. Idir
abdelhakim.idir@univ-msila.dz

[1] Department of Electrical Engineering, University Mohamed Boudiaf of M'sila, 28000 M'sila, Algeria

[2] Applied Automatics Laboratory, Faculty of Hydrocarbons and Chemistry, University of Boumerdes, Boumerdes, Algeria

[3] Department of Electrical Engineering, University of Bouira, 10000 Bouira, Algeria

[4] CNRS, LAPLACE Laboratory, UMR 5213, Toulouse, France

Published online: 23 January 2024

superiority of fractionalized PID controller with Matsuda approximation over classical ones.

Fractional differentiators and integrators are important in fractional filter-based signal processing and fractional feedback management of complex and chaotic systems [10]. A fractional-order system in the s-domain is an infinite-dimensional filter with an irrational continuous time transfer function.

In the literature, various approximation methods have been proposed to achieve low complexity and practical implementation of fractional derivative operators. Vinagre et al. [11] presented continuous models in the frequency domain and discrete models in the time domain. Khovanskii [12] and Vinagre et al. [11] proposed the continued fraction expansion (CFE) method, which yields an integer-order rational function that approximates fractional-order elements based on continued fraction expansion. Deniz et al. [13] presented the stability boundary locus (SBL) fitting method, which performs fitting of a rational transfer function to SBL curves of fractional-order elements or transfer functions within a desired frequency range. Wei et al. [14] proposed an algorithm for fixed pole approximation that results in smaller-order approximate models. Additionally, Bingi et al. [15] introduced a novel curve fitting-based approximation algorithm using the Sanathana-Koerner least square iterative. The Carlson methodology [17], Matsuda approximation method [18], Charef approximation method [19], Oustaloup approximation method [20] and the method provided by Xue et al. [21] are all well-known ways to produce the rational approximation.

The advantages of fractionalized PID based on the Harris Hawks optimization algorithm, which uses fractional-order filters to approximate integer-order transfers in the feedback control loop, are demonstrated in this study. The automation designer can apply the attributes and dynamics of fractional order to the rational system under consideration by inserting fractional-order integrators into the classical feedback control loop without modifying the overall equivalent closed loop transfer function.

In the airplane pitch angle control system, this study compares the responses of the traditional PID and the Oustaloup, Matsuda and Carlson fractionalized PID controllers. Some of these methods produce models with very high-order integer orders, allowing for the desired accuracy. Higher-order models, on the other hand, are difficult to realize, implement and simulate. This includes lowering the model's order, either by simplifying it or by computing a lower-order model, while retaining the important attributes and qualities of the original integer-order model.

The performance of the airplane pitch system can be further improved by using an ideal lower-order approximation of a fractionalized PID. Accordingly, this paper proposes a new reduced-order fractionalized PID (RFPID) controller based on the Harris Hawks optimization algorithm (HHOA) and approximation methods of Carlson, Matsuda and Oustaloup.

This paper's contribution to originality can be summarized as follows:

1. For the first time, a Carlson-based HHOA/reduced fractionalized PID controller was proposed.
2. For the first time, the efficiencies of appropriately designed Carlson HHOA/FPID, Matsuda HHOA/FPID and Oustaloup HHOA/FPID controllers for increasing aircraft system pitch angle performance were tested.
3. The performance of the proposed controllers approach has been compared in detail with the integer HHOA/PID controller [16] and integer HGSOA/PID controller [28] through several analyses, as these controllers with stated algorithms are the most recent techniques for determining optimal controller's gains.
4. The comparisons of transient and frequency responses clearly confirmed the performance of the proposed low-order fractionalized PID (RFPID) controller, as well as its superiority over current algorithms.

2 Mathematical model of the aircraft

During flight, the plane can be turned in three different directions. Yaw is rotation along the vertical axis, roll is rotation along the longitudinal axis, and pitch is rotation along the lateral axis. The axis intersects in the aircraft's gravity center.

Aircraft control is extremely difficult to model in a single model. However, some simplifications can be made below in the appropriate models provided for the control, resulting in an analysis of pitch control only.

- The drag, lift, thrust and weight forces are balanced in the x- and y directions if the aircraft is expected to be in a steady cruise at a constant speed and altitude.
- Any change in pitch angle should be assumed to have no effect on aircraft speed under all conditions for simplicity.

Figure 1 [22, 23] depicts the mathematical model for pitch angle.

The dynamic behavior of an aircraft is determined by the following set of relationships:

$$\frac{\mathrm{d}\alpha}{\mathrm{d}t} = \mu\Omega\sigma\left[-\left(C_L + C_D\right)\alpha + \frac{1}{\mu - C_L}q - \left(C_M \sin\gamma\right)\theta + C_L\right] \tag{1}$$

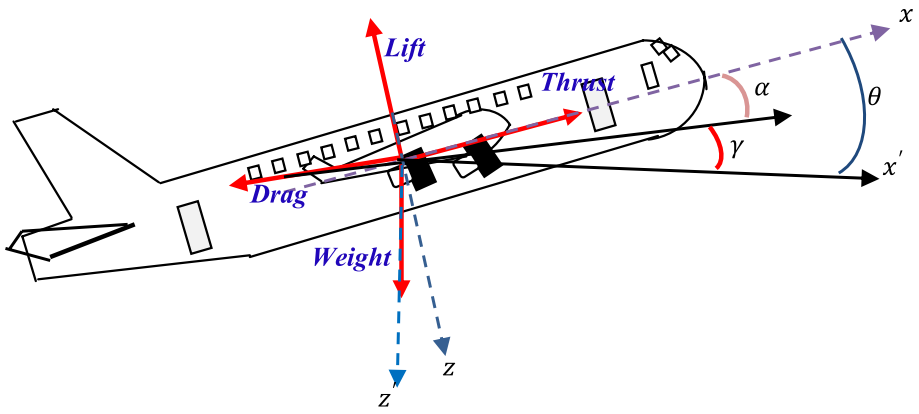

Fig. 1 Pitch control description

$$\frac{\mathrm{d}q}{\mathrm{d}t} = \frac{\mu\Omega}{2i_{yy}}\left[\left(C_M - \eta\left(C_L + C_D\right)\right)\alpha + \left(C_M + \sigma\left(1 - \mu C_L\right)\right)q + + \left(\eta C_w \sin\gamma\right)\delta\right] \tag{2}$$

$$\frac{\mathrm{d}\theta}{\mathrm{d}t} = \Omega q \tag{3}$$

with

$$\mu = \frac{\rho S\bar{c}}{4m}, \Omega = \frac{2\mathrm{U}}{\bar{c}}, \sigma = \frac{1}{1+\mu C_L}, \eta = \mu\sigma C_M$$

where α is the angle of attack, θ is the pitch angle, q is the pitch rate, γ is the flight path, δ is the elevator deflection angle, μ is the reduced mass of the aircraft, which represents the ratio of the air density (ρ) multiplied by the wing platform area (S) and the mean chord length ($\bar{c}$) to four times the mass of the aircraft (m), and Ω is the reduced frequency, a dimensionless quantity. It is the ratio of wing's oscillation frequency (2U) to the speed of sound ($\bar{c}$) in the surrounding fluid (typically air), U is the equilibrium flight speed and ($\bar{c}$) is the average chord length, which represents the distance between the airfoil's leading and trailing edges at a given spanwise point. σ represents the downwash factor (σ) of the aircraft, which is a dimensionless quantity used in aerodynamics to account for the effects of lift distribution on the aircraft's angle of attack. η represents the pitching moment coefficient of the aircraft, which is a dimensionless quantity used in aerodynamics to characterize the pitching moment generated by an aerodynamic body, such as an airfoil or wing. C_D, C_L, C_W and C_M are the coefficients for thrust, drag, lift, weight and pitch moment, respectively, and I_{yy} is the inertia normalized moment.

In this study, the coefficient of lift C_L is neglected; it means that the lift force generated by the wing or airfoil is assumed to be zero or not taken into account in the analysis or calculation. The following simplified modeling equations are generated by substituting the aircraft parameter values in Eqs. (1), (2) and (3):

$$\frac{\mathrm{d}\alpha(t)}{\mathrm{d}t} = -0.313\alpha(t) + 56.7q(t) + 0.232\theta(t) \tag{4}$$

$$\frac{\mathrm{d}q(t)}{\mathrm{d}t} = -0.0139\alpha(t) - 0.426q(t) + 0.0203\delta(t) \tag{5}$$

$$\frac{\mathrm{d}\theta(t)}{\mathrm{d}t} = 56.7q(t) \tag{6}$$

The following is the Laplace transform of the preceding equations (we assume that the initial conditions are null):

$$s\hat{\alpha}(s) = -0.313\hat{\alpha}(s) + 56.7Q(s) + 0.232\Theta(s) \tag{7}$$

$$sQ(s) = -0.0139\hat{\alpha}(s) - 0.426Q(s) + 0.0203\Delta(s) \tag{8}$$

$$s\Theta(s) = 56.7Q(s) \tag{9}$$

Finally, aircraft pitch angle transfer function is given in Eq. (10) [22].

$$G_P(s) = \frac{\Theta(s)}{\Delta(s)} = \frac{1.121s + 0.1774}{s^3 + 0.739s^2 + 0.9215s} \tag{10}$$

where $\Delta(s)$ is the elevator deflection and $\Theta(s)$ is the pitch angle.

The open-loop step response is shown in Fig. 2 with the input signal as step input $\delta = 0.2$. Based on the plot, it is clear that the open-loop response completely fails to meet the design objectives. In fact, the open-loop response is unstable. Determining the stability of a system entails examining the poles of its transfer function. The open-loop transfer function has a pole on the imaginary axis, indicating a system's free response will not grow unbounded but not decay to zero. However, a system with a pole on the imaginary axis can grow unbounded when given an input, even when the input is bounded. The pole at the origin acts like an integrator, causing the system's output to grow to infinity when given a step input.

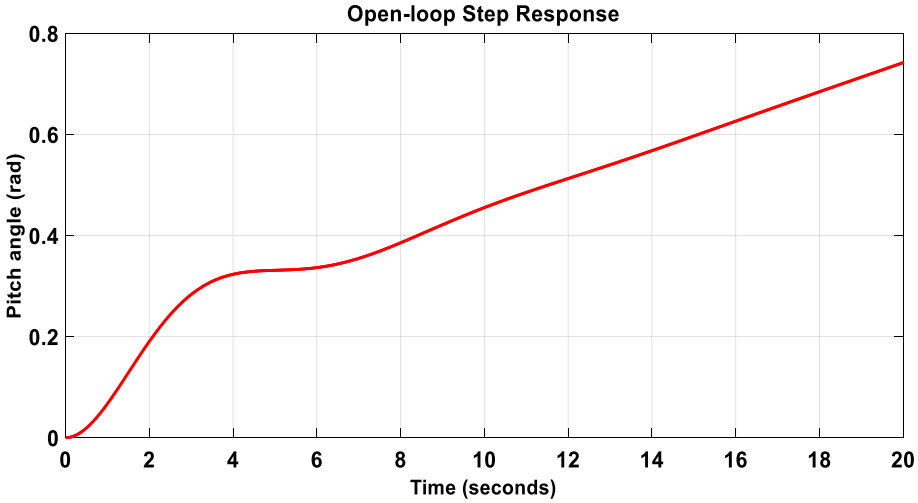

Fig. 2 Open-loop step response of aircraft pitch angle

3 Fractional-order approximation methods

The definition of the integro-differentiation operator D is given in many fractional-order (FO) calculus papers [24–26]:

$$aD_t^{\alpha} = \begin{cases} \frac{\mathrm{d}^{\alpha}}{\mathrm{d}t^{\alpha}}, & R(\alpha) > 0 \\ 1, & R(\alpha) = 0 \\ \int_a^t (\mathrm{d}\tau)^{-\alpha}, & R(\alpha) < 0 \end{cases} \tag{11}$$

where a represents the lower limit of integration, 't' represents the upper limit of integration, α represents the order of fractional differentiation or integration ($\alpha \in R$) and $R(\alpha)$ represents the real part of α.

Fractional-order systems are widely used in various fields, including control systems, signal processing, physics, biology and finance. They capture memory effects, better model fit, robustness against disturbances and uncertainties and can analyze fractal phenomena. Fractional-order calculus is closely related to fractal theory, allowing for better understanding of complex structures and non-locality in modeling systems with spatial or temporal interactions. These applications make fractional-order calculus an attractive choice for various applications.

Many definitions of the operation D can be found in the literature. Riemann–Liouville, Riesz, Weyl, Grünwald–Letnikov and Caputo [27–29] are among of them.

The Laplace transform of a fractional derivative of function f(t) with respect to t, denoted as $\mathcal{L}\left\{aD_t^{\alpha} f(t)\right\}$, is equal to s^{α} times the Laplace transform of $f(t)$, denoted as $F(s)$, where s is a complex variable.

3.1 Oustaloup filter approximation

To estimate fractional-order (FO) integrators and differentiators, Oustaloup's approximation approach is utilized [20]. An approximation of fractional operator s^{α} is the most important objective of Oustaloup's approximation [30].

$$G_f(s) = s^{\alpha}, (\alpha \in R) \tag{12}$$

The Oustaloup filter comes in a standard form:

$$G_f(s) = K \prod_{k=1}^{N} \frac{s + \omega_k'}{s + \omega_k} \tag{13}$$

where the zeros, poles and gain can be obtained from

$$\omega_k = \omega_b \omega_{ll}^{(2k-1+\gamma)/N}, \omega_k' = \omega_b \omega_{ll}^{(2k-1-\gamma)/N}, K = \omega_h^{\gamma} \tag{14}$$

For $k = 1, 2, \ldots, \mathrm{N}$ with

$$\omega_u = \sqrt{\frac{\omega_h}{\omega_b}} \tag{15}$$

where ω_b and ω_{h} are the desired lower and upper bound frequencies of the filter, respectively, γ is the order of derivative and N is the filter order.

3.2 Matsuda filter approximation

Matsuda's method is based on the continuous fraction technique (CFE) [18] to approximate an irrational function with a rational one. Assuming that the points selected are $s_k, k = 0, 1, 2, \ldots$, the approximation takes the following form:

$$G_f(s) = \alpha_0 + \frac{s - s_0}{\alpha_1 + \frac{s-s_1}{\alpha_2 + \frac{s-s_1}{\alpha_3 + \cdots}}} \tag{16}$$

where

$$\alpha_i = v_i(s_i), v_0(s) = G_f(s), v_{i+1}(s) = \frac{s - s_i}{v_i(s) - \alpha_i}. \tag{17}$$

3.3 Carlson filter approximation

The method suggested in [31] was obtained from an iterative estimate of the $\alpha - th$ root using a conventional Newton process. The method's beginning point is defined as

$$H(s) = G(s)^{\alpha} \tag{18}$$

The approximated rational function is obtained by setting the initial value to $H_0(s) = 1, \forall k = 1 \ldots N$:

$$H_k(s) = H_{k-1}(s)\frac{(1-\alpha)H_{k-1}(s)^{\frac{1}{\alpha}+(1+\alpha)G(s)}}{(1-\alpha)H_{k-1}(s)^{\frac{1}{\alpha}} + (1-\alpha)G(s)} \tag{19}$$

where the derivative is defined $G(s) = s$ and the integral is defined $G(s) = 1/s$.

- Using Oustaloup's approximation

$$G_{\alpha}(s) = G_{1-\alpha}(s) = G_{0.5}(s) = \frac{0.03162s^5 + 19.76s^4 + 1122s^3 + 6311s^2 + 3514s + 177.8}{s^5 + 197.6s^4 + 3549s^3 + 6311s^2 + 1111s + 17.78} \tag{20}$$

- Using Matsuda's approximation

$$G_{\alpha}(s) = G_{1-\alpha}(s) = G_{0.5}(s) = \frac{0.01386s^5 + 25.92s^4 + 1940s^3 + 11350s^2 + 5576s + 177.8}{s^5 + 313.5s^4 + 6383s^3 + 10910s^2 + 1458s + 7.797} \tag{21}$$

- Using Carlson's approximation

$$G_{\alpha}(s) = G_{1-\alpha}(s) = G_{0.5}(s) = \frac{0.1111s^6 + 4.074s^5 + 16.68s^4 + 19.11s^3 + 8.778s^2 + 1.704s + 0.1111}{s^6 + 10s^5 + 20.33s^4 + 14.37s^3 + 4.333s^2 + 0.5185s + 0.01235} \tag{22}$$

From these results, it is evident that when using any filter approximation method, it is essential to consider the specific requirements and characteristics of the filter you intend to design. This is because each method may yield different results in terms of accuracy, stability and performance.

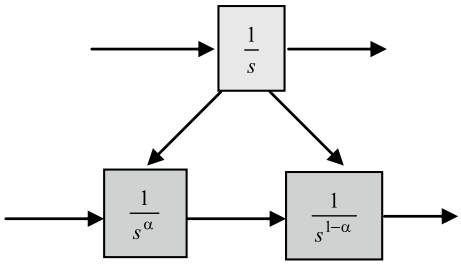

Fig. 3 Integral operator fractionalization

4 Frequency domain analysis of a fractionalized integrator

Consider the Laplace transform of the following integrator:

$$G(s) = \frac{1}{s} \tag{23}$$

Figure 3 shows the result of the classical integrator fractionalization Eq. (26).

$$\frac{1}{s} = \frac{1}{s^{\alpha}} \cdot \frac{1}{s^{1-\alpha}} \tag{24}$$

where α is a real number such that $0 < \alpha < 1$.

Using Oustaloup and Matsuda methods of approximation presented in Sect. 3 with the approximation parameters:$\omega_b = 0.01$ rad/s, $\omega_h = 1000$ rad/s, we get the approximated functions $G_{\alpha}(s)$ and $G_{1-\alpha}(s)$ given below (for $\alpha = 0.5$) It should be noted that, for the Carlson filter shown below, the actual order of the filter rises significantly as n increases; hence, $n = 2$ is commonly chosen. The integer-order integral operator $1/s$ and the product of fractional-order integral operators approximating filters $G_{\alpha}(s)$=$G_{1-\alpha}(s) = 1/s^{0.5}$ built utilizing singularity approximation methodologies are compared in the frequency domain in Fig. 4.

Figure 4 shows the filter's Bode diagram, which is placed on the exact responses of $1/s$. It can be seen that the Matsuda–Fujii filter has a broader fitting band. In addition, it is evident that this filter product $\left(1/s^{0.5}\right)X\left(1/s^{0.5}\right)$ provides a good approximation of the integral operator in the frequency interval of interest.

The frequency response fitting by Carlson and the Oustaloup filter are likewise good, as can be observed.

5 Fractionalized PID controller based on HHO algorithm

5.1 Fractionalized PID controller

The proposed fractionalization approach is examined in this study by analyzing its application to Eq. (10) transfer function of a feedback control aircraft system.

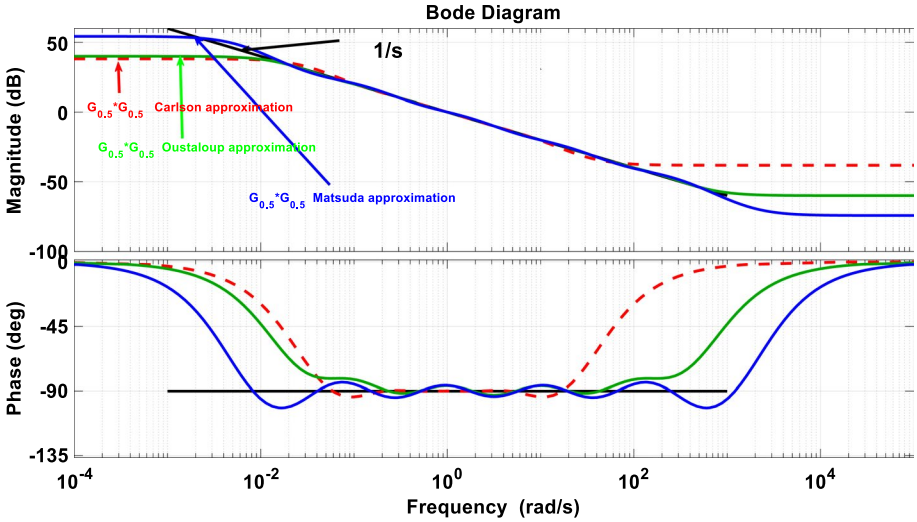

Fig. 4 Bode diagram comparison of the integration $1/s$ with the Oustaloup, Matsuda and Carlson approximations $G_{0.5}(s)XG_{0.5}(s)$

Figure 5 shows a feedback control loop with an HHOA based on a fractionalized PID controller.

In Fig. 6, θ_{ref} is the desired pitch angle, θ is the pitch angle, δ is deflection angle, $\left(K_p, K_i, K_d\right)$ are gains of fractionalized PID (proportional, integral and derivative, respectively), and α is the fractional order.

The traditional PID controller to be designed looks like this:

$$G_c(s) = K_p\left(1 + \frac{1}{T_i s} + T_d s\right) \tag{25}$$

where

$T_i = \frac{K_p}{K_i}$ and $T_d = \frac{K_d}{K_p}$.

The improvement fractionalization of the control system element modifies the PID control law, and the operator of integral $1/s$ is fractionalized as expressed in Eq. (28) and illustrated in Fig. 3, that is,

$$\frac{1}{s} = \frac{1}{s^{\alpha}} \cdot \frac{1}{s^{1-\alpha}}$$

The fractionalization of the traditional PID controller to be created looks like this [8, 9]:

$$G_c(s) = K_p\left(1 + \frac{1}{T_i s} + T_d s\right) = \frac{1}{s}\left(\frac{K_p T_i T_d s^2 + K_p T_i s + K_p}{T_i}\right)$$
$$= \frac{1}{s^{\alpha} s^{1-\alpha}}\left(\frac{K_p T_d T_i s^2 + K_p T_i s + K_p}{T_i}\right) \tag{26}$$

where $0 < \alpha < 1$.

5.2 Harris Hawks optimization algorithm (HHOA)

The Harris Hawks optimization algorithm (HHOA) is a population-based model that is inspired by nature [22]. This software is essentially a mathematical description of the searching behavior of Harris Hawks.

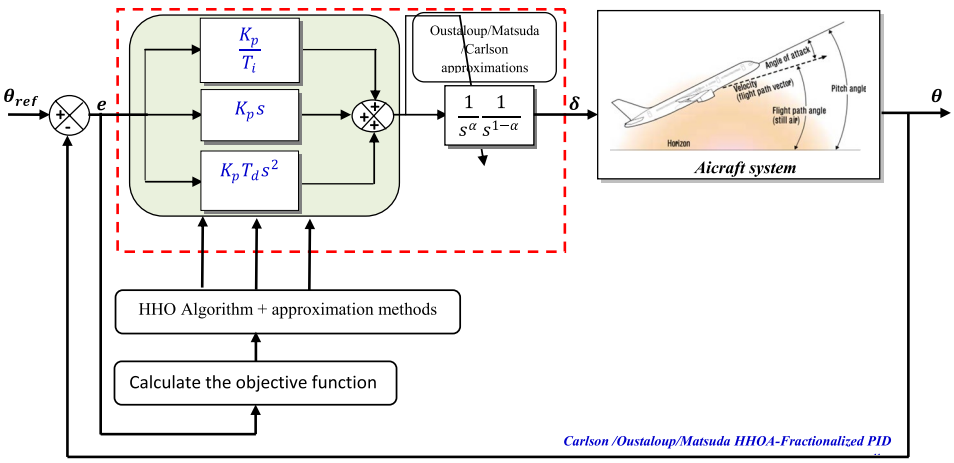

Fig. 5 The proposed HHOA-FPID approach using approximation methods for aircraft pitch angle control

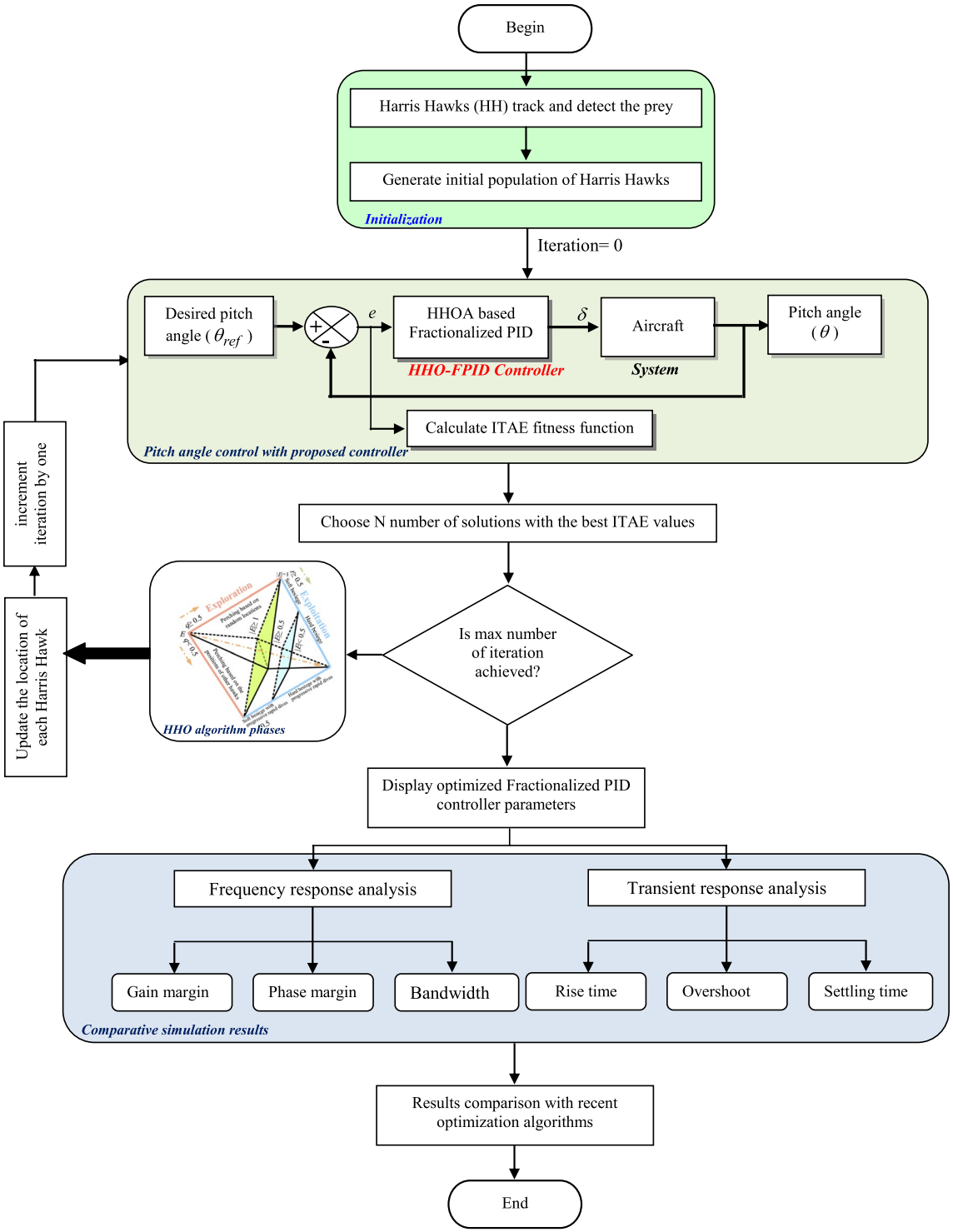

Fig. 6 Flowchart of the proposed design procedure for an aircraft pitch angle control

The various stages of Harris Hawks formulation are broken down into three main phases:

5.2.1 Exploration phase

This is the first step of the algorithm, during which Harris Hawks search for prey at random locations and employ a

wait-and-watch method to catch it:

$$X(t+1)=\begin{cases} X_{\text{rand}}(t)-r_1\left|X_{\text{rand}}(t)-2r_2X(t)\right| q\geq 0.5 \\ X_{\text{rab}}(t)-X_m(t)-r_3\left(L_b+r_4\left(U_b-L_b\right)\right) q<0.5 \end{cases} \tag{27}$$

where $X(t+1)$ is the Hawks' position in the next iteration, $X_{rabbit}(t)$ is the rabbit position, $X(t)$ is the vector of the Hawks' current position, $\left(r_1,r_2,r_3,r_4\right)$ are random numbers between (0, 1), $\left(L_b,U_b\right)$ are the lower and upper bounds of variables and $X_{\text{rand}}(t)$ is a randomly selected hawk from the current position.

The following formula is used to calculate the Hawks' average position:

$$X_m(t)=\frac{1}{N}\sum_{i=1}^{N}X_i(t) \tag{28}$$

where X_m is the mean of the current population of Hawks and N is the Hawks' total population.

5.2.2 Exploration to exploitation transition

This stage imitates a variety of Harris Hawk maneuvering strategies, which are based on the prey's energy level when fleeing (E). To demonstrate this behavior, imagine that the rabbit's energy comes from:

$$E=2E_0\left(1-\frac{t}{T_{\max}}\right) \tag{29}$$

where E,E_0 and $T_{\max}$ represent the escaping prey's energy, initial prey energy and the maximum number of iterations taken, respectively.

5.2.3 Exploitation phase

The final stage of the HHO algorithm can be divided into four distinct techniques. These tactics are determined by the energy level of the prey as well as the potential of escape.

Let's consider $r<0.5$ represents the successful escape chance of the prey, while $r\geq 0.5$ represents the unsuccessful escape.

For $r\geq 0.5$ and $|E|\geq 0.5$, a soft besiege will be performed in this case which is described by Eqs.(30) and (31).

$$X(t+1)=\Delta X(t)-E\left|JX_{\text{rabbit}}(t)-X(t)\right| \tag{30}$$

$$\Delta X(t)=X_{\text{rabbit}}(t)-X(t) \tag{31}$$

where $\Delta X(t)$ is the difference between the rabbit's position and the current place in iteration t and J is the rabbit's random jump strength.

- For $r\geq 0.5$ and $|E|<0.5$, a hard besiege will be performed in this case which is described by Eq. (32).

$$X(t+1)=X_{\text{rabbit}}(t)-E|\Delta X(t)| \tag{32}$$

- For $r<0.5$ and $|E|\geq 0.5$, a soft besiege with progressive rapid drive will be performed in this case which is described by Eqs. (33) and (34).

$$Y_1=X_{\text{rabbit}}(t)-E\left|JX_{\text{rabbit}}-X(t)\right| \tag{33}$$

$$Z_1=Y_1+S\times LF(D) \tag{34}$$

where D is the problem dimension, S is a size random vector $1\times D$ and LF is levy flight function.

Therefore, the position update is fulfilled using Eq. (35).

$$X(t+1)=\begin{cases} Y_1, & \text{if } F\left(Y_1\right)<F(X(t) \\ Z_1, & \text{if } F\left(Z_1\right)<F(X(t)) \end{cases} \tag{35}$$

- For r and $|E|$ having values smaller than 0.5, a hard besiege with progressive rapid drive will be performed in this case which is described by Eqs. (36)–(38).

$$X(t+1)=\begin{cases} Y_2, & \text{if } F\left(Y_2\right)<F(X(t)) \\ Z_2, & \text{if } F\left(Z_2\right)<F(X(t)) \end{cases} \tag{36}$$

Y_2 and Z_2 are obtained using (33) and (34), respectively.

$$Y_2=X_{\text{rabbit}}(t)-E\left|JX_{\text{rabbit}}-X(t)\right| \tag{37}$$

$$Z_2=Y_2+S\times LF(D) \tag{38}$$

6 Carlson/Oustaloup/Matsuda HHO-fractionalized PID approach of aircraft system control

The initialization phase of the optimal gains of the PID controller with the HHO algorithm has started with the integration of the advanced MATLAB/Simulink model for aircraft pitch control with the HHO algorithm and approximation methods in the initialization phase. The PID controller's gains were assigned to a vector of real values representing each Harris Hawk in the population, which needed to be optimized. The population consisted of N Harris Hawks and their opposing forces, which were produced randomly. Figure 6 depicts a detailed flowchart of the suggested design approach.

Accordingly, for each Harris Hawk, a time-domain simulation of the aircraft's pitch angle control system was

performed with the proposed fractionalized PID controller and unit feedback, and response curves of the pitch angle of the aircraft system were obtained along with the integral Time absolute error (ITAE) criteria.

The ITAE performance criterion was chosen for this investigation because it allows a good comparison with the references [22, 32]. Equation (39) shows the ITAE objective function:

$$J\left(K_p, K_i, K_d\right) = \int_0^{t_{sim}} t|e(t)|\mathrm{d}t \tag{39}$$

J stands for performance criteria. It indicates the degree to which the controlled object is similar to the reference model. Here $e(t)$ represents the difference between the set point and the controlled variable, and t is the time.

Table 1 lists the parameters of the proposed HHO algorithm. The HHO algorithm is used to construct a PID controller for the system model $G_p(s)$ shown in Eq. (10) with the following PID parameters: $K_p = 55.27$, $K_i = 51.40$, and $K_d = 90$. The closed-loop transfer function of an aircraft system with fractionalized PID and unity feedback is obtained as:

$$G_{\mathrm{CLFPID}}(s) = \frac{G_{\mathrm{HHO-FPID}}(s)^* G_p(s)}{1 + G_{\mathrm{HHO-FPID}}(s) * G_p(s)} \tag{40}$$

As a result, the closed-loop transfer function is 'fractionalized' as shown in Eq. (24), with integrator fractional order $\alpha = 0.1$ approximated using the methods of Carlson, Matsuda and Oustaloup with the approximation parameters: $\omega_b = 0.01$ rad/s, $\omega_h = 1000$ rad/s and unity feedback for the HHO algorithm is given by:

$$G_{CL\,\mathrm{FPID-Oust}}(s) = \frac{\begin{array}{c}0.1047s^{13} + 145s^{12} + 5.18e4s^{11} + 5.272e6s^{10} + 1.74e08s^9 + 1.807e09s^8 + \\ 6.761e09s^7 + 1.044e10s^6 + 9.306e09s^5 + 5.305e09s^4 + 1.446e09s^3 + \\ 2.404e08s^2 + 1.481e07s + 2.883e05\end{array}}{\begin{array}{c}1.105s^{13} + 583.6s^{12} + 1.015e5s^{11} + 6.89e6s^{10} + 1.914e08s^9 + 1.871e09s^8 + \\ 6.865e09s^7 + 1.054e10s^6 + 9.366e09s^5 + 5.332e09s^4 + 1.648e09s^3 + \\ 2.404e08s^2 + 1.481e07s + 2.883e05\end{array}} \tag{41}$$

Table 1 Parameters of HHOA-PID for solving optimization problem

Number of hawks (population size)	50
Maximum iteration number	40
Constant of levy flight function	1.5
Lower bound for $[K_p; K_i; K_d]$	[0.01;0.01;0.01]
Upper bound for $[K_p; K_i; K_d]$	[100;100;100]
Dimension for optimization problem	3
Time of simulation	1 s

Table 2 Approximation order using Carlson method (Iteration 1)

$G_\alpha(s) = \frac{1}{s^\alpha}$	Carlson's approximation	$G_\alpha(s) = \frac{1}{s^\alpha}$	Carlson's approximation
$G_{0.1}(s)$	$\frac{s+1.222}{1.222s+1}$	$G_{0.6}(s)$	$\frac{s^2+4.222s+3.666}{3.667s^2+4.222s+0.9999}$
$G_{0.2}(s)$	$\frac{s+1.5}{1.5s+1}$	$G_{0.7}(s)$	$\frac{s^2+4.5s+4.5}{4.5s^2+4.5s+0.9999}$
$G_{0.3}(s)$	$\frac{s^2+2.722s+1.833}{1.833s^2+2.722s+1}$	$G_{0.8}(s)$	$\frac{s^3+5.722s^2+9.999s+5.499}{5.5s^3+10s^2+5.722s+1}$
$G_{0.4}(s)$	$\frac{s^2+3s+2.25}{2.25s^2+3s+1}$	$G_{0.9}(s)$	$\frac{s^3+6s^2+11.25s+6.75}{6.75s^3+11.25s^2+6s+1}$
$G_{0.5}(s)$	$\frac{s+3}{3s+1}$	–	–

Table 3 Approximation order using Matsuda

$G_\alpha(s) = \frac{1}{s^\alpha}$	Matsuda's approximation
$G_{0.1}(s)$	$\frac{0.4342s^5+347.1s^4+15130s^3+54070s^2+16070s+281.8}{s^5+570.1s^4+19190s^3+53670s^2+12320s+154.1}$
$G_{0.2}(s)$	$\frac{0.1877s^5+180.5s^4+8971s^3+36260s^2+12240s+281.8}{s^5+487.1s^4+14440s^3+35710s^2+7186s+74.71}$
$G_{0.3}(s)$	$\frac{0.0803s^5+94.29s^4+5357s^3+24490s^2+9372s+223.9}{s^5+418.6s^4+10940s^3+23930s^2+4212s+35.87}$
$G_{0.4}(s)$	$\frac{0.0338s^5+49.41s^4+3216s^3+16630s^2+7214s+199.5}{s^5+361.6s^4+8336s^3+16120s^2+2476s+16.94}$
$G_{0.5}(s)$	$\frac{0.01386s^5+25.92s^4+1940s^3+11350s^2+5576s+177.8}{s^5+313.5s^4+6383s^3+10910s^2+1458s+7.797}$
$G_{0.6}(s)$	$\frac{0.005466s^5+13.6s^4+1174s^3+7778s^2+4324s+158.5}{s^5+272.8s^4+4908s^3+7405s^2+858.3s+3.449}$
$G_{0.7}(s)$	$\frac{0.00202s^5+7.128s^4+712s^3+5348s^2+3363s+141.3}{s^5+238.1s^4+3786s^3+5040s^2+504.6s+1.43}$
$G_{0.8}(s)$	$\frac{0.0006621s^5+3.723s^4+432.7s^3+3687s^2+2622s+125.9}{s^5+208.3s^4+2929s^3+3437s^2+295.8s+0.526}$
$G_{0.9}(s)$	$\frac{0.0001622s^5+1.936s^4+263.4s^3+2548s^2+2049s+112.2}{s^5+182.6s^4+2271s^3+2347s^2+172.5s+0.1446}$

Table 4 Approximation order using Oustaloup

$G_\alpha(s)=\frac{1}{s^\alpha}$	Oustaloup's approximation
$G_{0.1}(s)$	$\frac{0.5012s^5+197.6s^4+7081s^3+25120s^2+8826s+281.8}{s^5+313.2s^4+8914s^3+25120s^2+7011s+177.8}$
$G_{0.2}(s)$	$\frac{0.2512s^5+111.1s^4+4468s^3+17790s^2+7011s+251.2}{s^5+279.1s^4+7081s^3+17790s^2+4423s+100}$
$G_{0.3}(s)$	$\frac{0.1259s^5+62.48s^4+2819s^3+12590s^2+5569s+223.9}{s^5+248.7s^4+5624s^3+12590s^2+2791s+56.23}$
$G_{0.4}(s)$	$\frac{0.0631s^5+35.14s^4+1779s^3+8914s^2+4423s+199.5}{s^5+221.7s^4+4468s^3+8914s^2+1761s+31.62}$
$G_{0.5}(s)$	$\frac{0.03162s^5+19.76s^4+1122s^3+6311s^2+3514s+177.8}{s^5+197.6s^4+3549s^3+6311s^2+1111s+17.78}$
$G_{0.6}(s)$	$\frac{0.01585s^5+11.11s^4+708.1s^3+4468s^2+2791s+158.5}{s^5+176.1s^4+2819s^3+4468s^2+701.1s+10}$
$G_{0.7}(s)$	$\frac{0.007943s^5+6.248s^4+446.8s^3+3163s^2+2217s+141.3}{s^5+156.9s^4+2239s^3+3163s^2+442.3s+5.623}$
$G_{0.8}(s)$	$\frac{0.003981s^5+3.514s^4+281.9s^3+2239s^2+1761s+125.9}{s^5+139.9s^4+1779s^3+2239s^2+279.1s+3.162}$
$G_{0.9}(s)$	$\frac{0.001995s^5+1.976s^4+177.9s^3+1585s^2+1399s+112.2}{s^5+124.7s^4+1413s^3+1585s^2+176.1s+1.778}$

parameters:$\omega_b = 0.01$ rad/s, $\omega_h = 1000$ rad/s and filter order $N = 5$.

Some of these methods produce very high-order integer-order models, allowing for the desired accuracy. Higher-order models, on the other hand, are difficult to realize, implement and simulate. This includes decreasing the model's order, either by simplifying it or computing a lower-order model, while keeping the original integer-order model's important traits and qualities.

Figure 7 shows the error signal for model reduction, where the original model is given by

$$G(s) = \frac{b_1 s^{n-1} + \cdots + b_{n-1}s + b_0}{s^n + a_1 s^{n-1} + \cdots + \alpha_{n-1}s + a_n} \tag{44}$$

$$G_{CL\,\mathrm{FPID-Mats}}(s) = \frac{\begin{array}{c}0.007376s^{13} + 93.93s^{12} + 8.267e4s^{11} + 1.282e7s^{10} + 5.305e08s^9 + \\ 6.009e09s^8 + 2.273e10s^7 + 3.361e10s^6 + 2.882e10s^5 + 1.558e10s^4 + \\ 4.331e09s^3 + 5.287e08s^2 + 2.388e07s + 2.883e05\end{array}}{\begin{array}{c}1.007s^{13} + 847.4s^{12} + 2.088e5s^{11} + 1.777e7s^{10} + 5.889e08s^9 + \\ 6.223e09s^8 + 2.306e10s^7 + 3.392e10s^6 + 2.9e10s^5 + 1.562e10s^4 + 4.333e09s^3 + \\ 5.287e08s^2 + 2.388e07s + 2.883e05\end{array}} \tag{42}$$

$$G_{\mathrm{CLFPID-Carlson}}(s) = \frac{104.7s^7 + 835.9s^6 + 2591s^5 + 4135s^4 + 3846s^3 + 2241s^2 + 755.8s + 75.21}{113s^7 + 862.5s^6 + 2632s^5 + 4175s^4 + 3869s^3 + 2248s^2 + 756.7s + 75.21} \tag{43}$$

The HHO algorithm-based closed-loop system with fractionalized PID has a high order. As a result, the memory capacity of the fractionalized PID controller will be lowered to fit better inside the correction loop.

Similarly, for different integrator fractional orders $\alpha = 0.2$, $\alpha = 0.3$, $\alpha = 0.4$, and $\alpha = 0.5$, the integer-order approximation models given in Tables 2, 3, 4 may be utilized to determine the closed loop transfer functions of the HHOA-based fractionalized PID using Carlson, Matsuda and Oustaloup approximation methods.

Tables 2, 3 and 4 show a list of integer-order approximation models found by Carlson, Matsuda and Oustaloup approximation methods using these

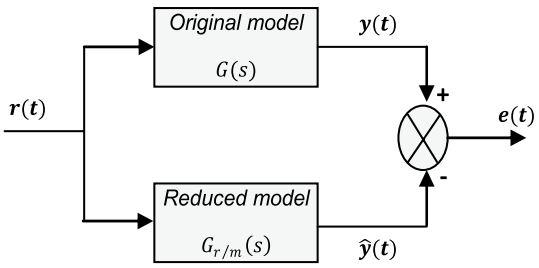

Fig. 7 Error signal for model reduction

As indicated below [32], our current goal is to find a low-order approximation integer-order model.

$$G_{r/m}(s) = \frac{\beta_1 s^{\mathrm{r}} + \cdots + \beta_r s + \beta_{r+1}}{s^{\mathrm{m}} + \alpha_1 s^{m-1} + \cdots + \alpha_{m-1}s + \alpha_m} \tag{45}$$

The error signal's Laplace transform can be represented as:

$$E(s) = G(s) - G_{r/m}(s) \tag{46}$$

where $R(s)$ is the Laplace transform of the input signal $r(t)$.

An objective function for minimizing the $H2-$ norm of the reduction error signal is as follows:

$$J = \min_{\theta} \hat{G}(s) - G_{r/m}(s)_2 \tag{47}$$

where θ the parameters are tuned so that:

$$\theta = \left[\beta_1, \ldots, \beta_r, \alpha_1, \ldots, \alpha_m\right] \tag{48}$$

where J is the criterion of performance and $G_{r/m}(s)$ is the reduced-order model.

As a result, the low-order closed loop transfer function of high-order closed loop given in Eqs. 41 − 43 with the resultant PID controller 'fractionalized' with integrator

Table 5 Transfer function of proposed fractionalized PID controllers

Controller type	Carlson RFPID $G_{CL\_Carlson-RFPID}(s)$	Matsuda RFPID $G_{CL\_Matsuda-RFPID}(s)$	Oustaloup RFPID $G_{CL\_Oustaloup-RFPID}(s)$
Original* model Test 1 [0.1 0.9]	$\frac{176.1s^3+134.1s^2+116s+15.34}{s^4+177.1s^3+135.2s^2+116.2s+15.34}$	$\frac{124s^3+94.42s^2+81.65s+10.8}{s^4+124.7s^3+95.34s^2+81.65s+10.8}$	$\frac{109.8s^3+83.62s^2+72.31s+9.56}{s^4+110.5s^3+84.55s^2+72.32s+9.56}$
Original model Test 2 [0.2 0.8]	$\frac{176.1s^3+134.1s^2+116s+15.34}{s^4+177s^3+135.2s^2+116.2s+15.34}$	$\frac{142.2s^3+108.3s^2+93.67s+12.38}{s^4+143s^3+109.2s^2+93.67s+12.38}$	$\frac{113.9s^3+86.78s^2+75.04s+9.922}{s^4+114.7s^3+87.71s^2+75.05s+9.922}$
Original model Test 1 [0.3 0.7]	$\frac{176.1s^3+134.1s^2+116s+15.34}{s^4+177s^3+135.2s^2+116.2s+15.34}$	$\frac{157s^3+119.6s^2+103.4s+13.67}{s^4+157.7s^3+120.5s^2+103.4s+13.67}$	$\frac{117s^3+89.13s^2+77.07s+10.19}{s^4+117.8s^3+90.06s^2+77.08s+10.19}$
Original model Test 1 [0.4 0.6]	$\frac{176.1s^3+134.1s^2+116s+15.34}{s^4+177.1s^3+135.2s^2+116.2s+15.34}$	$\frac{166.5s^3+126.8s^2+109.6s+14.5}{s^4+167.2s^3+127.7s^2+109.6s+14.5}$	$\frac{118.9s^3+90.59s^2+78.34s+10.36}{s^4+119.7s^3+91.52s^2+78.35s+10.36}$
Original model Test 1 [0.5 0.5]	$\frac{171.1s^3+130.3s^2+112.7s+14.9}{s^4+172s^3+131.4s^2+112.9s+14.9}$	$\frac{169.7s^3+129.2s^2+111.8s+14.78}{s^4+170.4s^3+130.2s^2+111.8s+14.78}$	$\frac{109.8s^3+83.62s^2+72.31s+9.56}{s^4+110.5s^3+84.55s^2+72.32s+9.56}$

Table 6 Optimized PID controller parameters

Controller	*Kp*	*Ki*	*KdKd*
HHOA-based PID [16]	55.2698	51.4031	90.9434
HGSOA-based PID [28]	69.7726	3.6054	95.1465

fractional order derived using Oustaloup, Matsuda and Carlson approaches becomes:

$$G_{CL_{\text{RFPID}-O\ \text{Ustaloup}}}(s) = \frac{109.8s^3 + 83.62s^2 + 72.31s + 9.56}{s^4 + 110.5s^3 + 84.55s^2 + 72.32s + 9.56} \tag{49}$$

$$G_{CL_{\text{RFPID}-\text{Matsuda}}}(s) = \frac{124s^3 + 94.2s^2 + 81.65s + 10.8}{s^4 + 124.7s^3 + 95.34s^2 + 81.65s + 10.8} \tag{50}$$

$$G_{CL_{\text{RFPID}-\text{Carison}}}(s) = \frac{176.1s^3 + 134.1s^2 + 116s + 15.34}{s^4 + 177.1s^3 + 135.2s^2 + 116.2s + 15.34} \tag{51}$$

Therefore, closed-loop transfer functions of the HHOA-based reduced-order fractionalized PID controller with Oustaloup, Matsuda and Carlson approximation methods for different integrator fractional orders $\alpha = 0.2$, $\alpha = 0.3$, $\alpha = 0.4$, and $\alpha = 0.5$ applied to aircraft system are listed in Table 5. The reduced models are all of order 3/4.

6.1 Original model

$$G_{\text{HHOA/FPID}}(s) = \frac{\Theta_{\text{des}}(s)}{\Theta_{\text{ref}}(s)} = \frac{\left(K_d s^2 + K_p s + K_i\right)(1.121s + 0.1774)}{s^{\alpha}s^{1-\alpha}\left(s^3 + 0.739s^2 + 0.9215s\right) + \left(K_d s^2 + K_p s + K_i\right)(1.121s + 0.1774)}$$

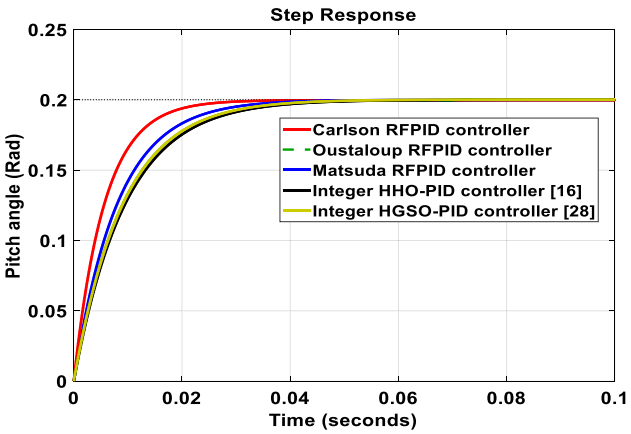

Fig. 8 Pitch angle changing curves for test 1: $\alpha = 0.1$

7 Comparative simulation results and discussion

The algorithm's performance in directing the pitch angle response of an aircraft system given in Eq. (10) is verified through the following simulations. The simulations were developed using MATLAB/SIMULINK software.

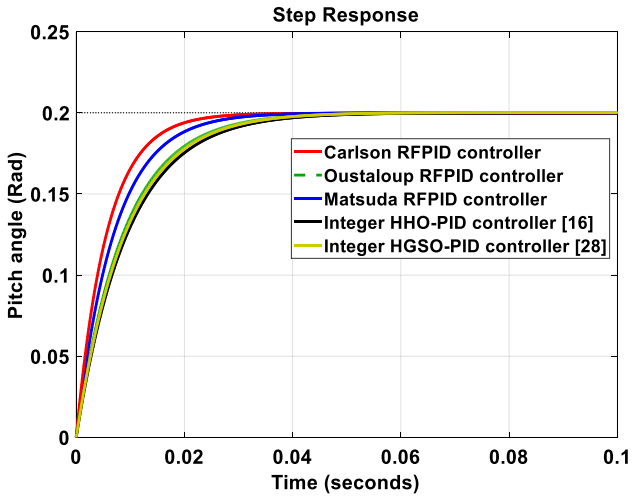

Fig. 9 Pitch angle changing curves for test 2: $\alpha = 0.2$

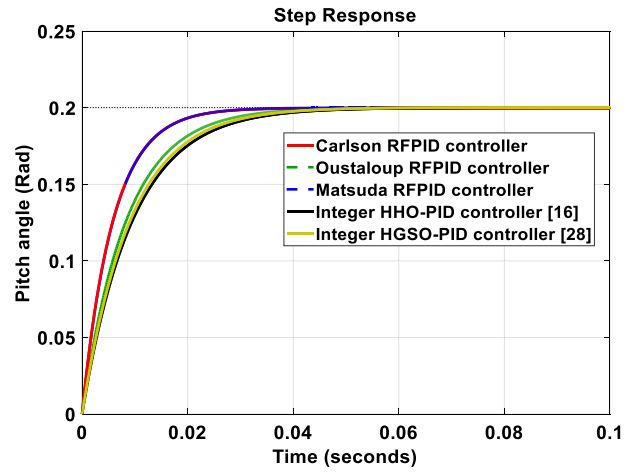

Fig. 10 Pitch angle changing curves for test 3:$\alpha = 0.5$

The simulations of the transient response and frequency response were carried out using the specified environment. The simulation results of various analyses obtained by using the proposed reduced-order fractionalized PID controllers, acquired through various approximation methods, are compared with other recent approaches such as HHO [16] and HGSO [28] used for optimizing the classical PID controller. HHO is explained in subsect. 5.B, and Henry gas solubility optimization (HGSO) is an optimization algorithm that utilizes Henry's law to mimic the behavior of gas molecules dissolving in liquids. It employs exploration and exploitation principles to find optimal solutions in problem spaces, guiding the search for optimal solutions [9, 28].

Table 7 Comparative analysis of transient response performance [$\alpha = 0.1 - \alpha = 0.9$]

Controller	OS, %	t_r	$t_s \pm 2\%$
Carlson RFPID controller [Proposed]	**0.0000**	**0.0125**	**0.0225**
Matsuda RFPID controller [Proposed]	**0.0000**	0.0177	0.0315
Oustaloup RFPID controller [Proposed]	**0.0000**	0.0200	0.0356
Integer HHO/PID [16]	**0.0000**	0.0210	0.0373
Integer HGSOA/PID [28]	**0.0000**	0.0200	0.0352

Bold values indicate the better results than other controllers

7.1 Comparison of overshoot, rising time and settling time

Table 6 shows the PID controller settings that correlate to the ITAE criterion function's minimum value for a variety of controllers selected for fair comparison.

Using these parameters, the transfer functions of HHOA-based PID and HGSOA-based PID controllers are given in Eqs. (52)–(53).

$$G_{CL_{\text{HHOA-PID}}}(s) = \frac{104.7s^3 + 79.75s^2 + 68.97s + 9.118}{s^4 + 105.4s^3 + 80.67s^2 + 68.97s + 9.118} \quad (52)$$

$$G_{CL_{\text{HGSOA-PID}}}(s) = \frac{109.5s^3 + 79.18s^2 + 16.45s + 0.6282}{s^4 + 110.3s^3 + 98.11s^2 + 16.45s + 0.6282} \quad (53)$$

To compare the performances of the proposed approaches (HHOA/RFPID) for aircraft pitch angle control with other existing approaches such as HHOA/PID[16] and HGSO/PID[28], a comparative stability analysis was performed in the time and frequency domains; using an input reference of $\theta_{\text{ref}} = 0.1$ rad.

Figures 8, 9 and 10 compare the set point following of aircraft pitch angle obtained by the three proposed controllers and integer HHOA/PID [16] and HGSOA/PID [28] controllers for different integrators fractional order $\alpha = 0.1$, $\alpha = 0.2$ and $\alpha = 0.5$ of the fractionalized PID, respectively.

The suggested Carlson HHOA/RFPID controller has superior time response than others, as shown in Fig. 8; except for $\alpha = 0.5$, the performance of Carlson HHOA/RFPID and Matsuda HHOA/RFPID is very close.

Tables 7, 8, 9, 10 and 11 compare the transient response study simulation study for all integral fractional operators (Five tests) in terms of maximum percentage overshoot, rising time (for 10–90% tolerance) and settling time (for 2% tolerance) obtained by the RFPID controllers with different approximation methods and other controllers.

The pitch angle of the aircraft system with the proposed Carlson HHOA/RFPID exhibited the fastest settling and rise times without overshoot, as shown in Tables 7, 8, 9, 10.

Table 8 Comparative analysis of transient response performance [$\alpha = 0.2 - \alpha = 0.8$]

Controller	OS, %	t_r	$t_s \pm 2\% t_s \pm 2\%$
Carlson RFPID controller [Proposed]	**0.0000**	**0.0124**	**0.0224**
Matsuda RFPID controller [Proposed]	**0.0000**	0.0154	0.0275
Oustaloup RFPID controller [Proposed]	**0.0000**	0.0193	0.0343
Integer HHO/PID [16]	**0.0000**	0.0210	0.0373
Integer HGSOA/PID [28]	**0.0000**	0.0200	0.0352

Bold values indicate the better results than other controllers

Table 9 Comparative analysis of transient response performance [$\alpha = 0.3 - \alpha = 0.7$]

Controller	OS, %	t_r	$t_s \pm 2\%$
Carlson RFPID controller [Proposed]	**0.0000**	**0.0125**	**0.0225**
Matsuda RFPID controller [Proposed]	0.0008	0.0140	0.0249
Oustaloup RFPID controller [Proposed]	**0.0000**	0.0188	0.0334
Integer HHO/PID [16]	**0.0000**	0.0210	0.0373
Integer HGSOA/PID [28]	**0.0000**	0.0200	0.0352

Bold values indicate the better results than other controllers

Table 10 Comparative analysis of transient response performance [$\alpha = 0.4 - \alpha = 0.6$]

Controller	OS, %	t_r	$t_s \pm 2\%$
Carlson RFPID controller [Proposed]	**0.0000**	0.0125	0.0224
Matsuda RFPID controller [Proposed]	0.0008	0.0132	0.0235
Oustaloup RFPID controller [Proposed]	**0.0000**	0.0185	0.0329
Integer HHO/PID [16]	**0.0000**	0.0210	0.0373
Integer HGSOA/PID [28]	**0.0000**	0.0200	0.0352

Bold values indicate the better results than other controllers

Table 11 Comparative analysis of transient response performance [$\alpha = 0.5 - \alpha = 0.5$]

Controller	OS, %	t_r	$t_s \pm 2\%$
Carlson RFPID controller [Proposed]	**0.0000**	**0.0129**	0.0231
Matsuda RFPID controller [Proposed]	0.0008	**0.0129**	**0.0230**
Oustaloup RFPID controller [Proposed]	**0.0000**	0.0200	0.0356
Integer HHO/PID [16]	**0.0000**	0.0210	0.0373
Integer HGSOA/PID [28]	**0.0000**	0.0200	0.0352

Bold values indicate the better results than other controllers

The Carlson HHOA/RFPID controller design approach proposed not only outperforms the Matsuda HHOA/RFPID and Oustaloup HHOA/RFPID controller design approaches, but also other controller design approaches such as integer HHOA/PID [16] and integer HGSO/PID [28] in terms of transient stability, fast damping

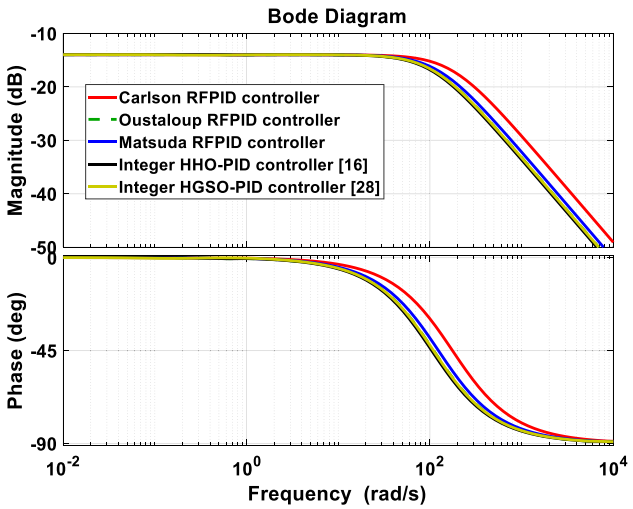

Fig. 11 Bode graphs comparing different controller designs for test 1: $\alpha = 0.1$.

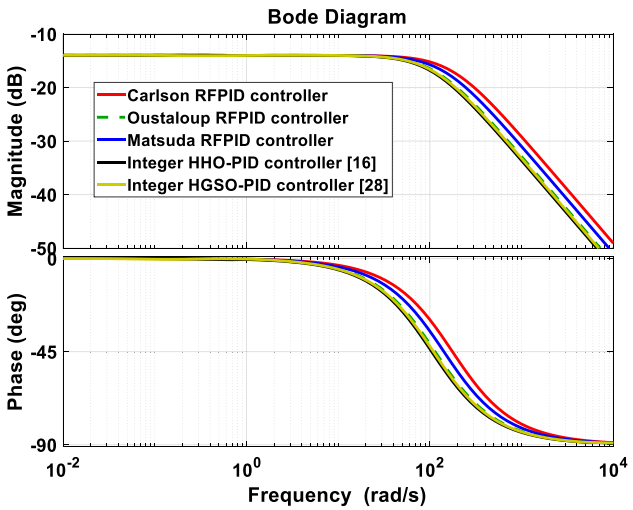

Fig. 12 Bode graphs comparing different controller designs for test 2:$\alpha = 0.2$.

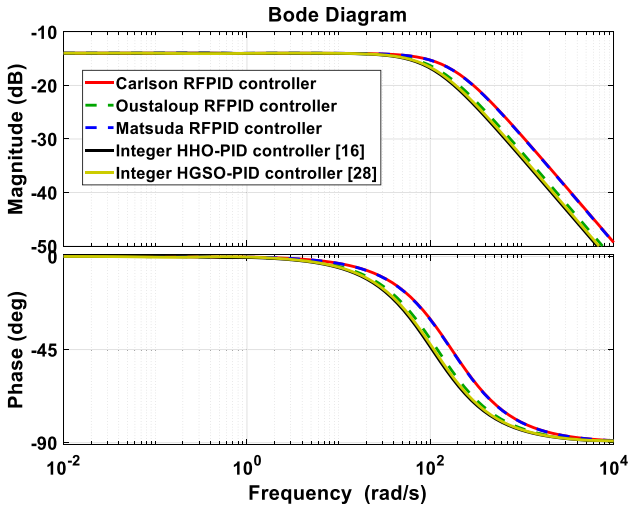

Fig. 13 Bode graphs comparing different controller designs for test 5:$\alpha = 0.5$.

Table 12 Comparative analysis of transient response performance [$\alpha = 0.1 - \alpha = 0.9$]

Controller	G_m[dB]	φ_m[°]	Bw [Hz]
Carlson RFPID controller [proposed]	∞	180	**175.5093**
Matsuda RFPID controller [proposed]	∞	179.5987	123.6927
Oustaloup RFPID controller [proposed]	∞	179.5575	109.5320
Integer HHO/PID [16]	∞	179.5244	104.4835
Integer HGSOA/PID [28]	∞	177.3060	109.4146

Bold values indicate the better results than other controllers

Table 13 Comparative analysis of transient response performance [$\alpha = 0.2 - \alpha = 0.8$]

Controller	G_m[dB]	φ_m[°]	Bw [Hz]
Carlson RFPID controller [proposed]	∞	180	**175.5061**
Matsuda RFPID controller [proposed]	∞	179.6507	141.8900
Oustaloup RFPID controller [proposed]	∞	179.5739	113.6756
Integer HHO/PID [28]	∞	179.5244	104.4835
Integer HGSOA/PID [28]	∞	177.3060	109.4146

Bold values indicate the better results than other controllers

characteristics and minimum overshoot. The rise and settling times of Carlson HHOA/RFPID and Matsuda HHOA/RFPID controllers are nearly identical, with minor changes, as shown in Table 11.

Table 14 Comparative analysis of transient response performance [$\alpha = 0.3 - \alpha = 0.7$]

Controller	G_m[dB]	φ_m[°]	Bw [Hz]
Carlson RFPID controller [proposed]	∞	180	**175.5093**
Matsuda RFPID controller [proposed]	∞	179.6840	156.6461
Oustaloup RFPID controller [proposed]	∞	179.5854	116.7515
Integer HHO/PID [16]	∞	179.5244	104.4835
Integer HGSOA/PID [28]	∞	179.5244	104.4835

Bold values indicate the better results than other controllers

Table 15 Comparative analysis of transient response performance [$\alpha = 0.4 - \alpha = 0.6$]

Controller	G_m[dB]	φ_m[°]	Bw [Hz]
Carlson RFPID controller [proposed]	∞	180	**175.5093**
Matsuda RFPID controller [proposed]	∞	179.7023	166.0820
Oustaloup RFPID controller [proposed]	∞	179.5923	118.6640
Integer HHO/PID [16]	∞	179.5244	104.4835
Integer HGSOA/PID [28]	∞	179.5244	104.4835

Bold values indicate the better results than other controllers

Table 16 Comparative analysis of transient response performance [$\alpha = 0.5 - \alpha = 0.5$]

Controller	G_m[dB]	φ_m[°]	Bw [Hz]
Carlson RFPID controller [proposed]	∞	180	**170.5491**
Matsuda RFPID controller [proposed]	∞	179.7080	169.2970
Oustaloup RFPID controller [proposed]	∞	179.5575	109.5320
Integer HHO/PID [16]	∞	179.5244	104.4835
Integer HGSOA/PID [28]	∞	179.5244	104.4835

Bold values indicate the better results than other controllers

7.2 Comparison of frequency domain analyses

Bode graphs with various controller configurations are compared in Figs. 11, 12, 13.

The results of the comparative frequency response performance analysis are presented in Tables 12, 13, 14, 15, 16, which includes gain margin (in decibels), phase margin (in degrees) and bandwidth (in Hertz).

As shown in Tables 12, 13, 14, 15 and 16, the aircraft system with the proposed Carlson HHOA/RFPID controller has the maximum phase margin 180°, while the proposed Matsuda and Oustaloup /HHOA-RFPID, integer HHO/PID

[16] and integer HGSOA/PID [28] controller have an acceptable phase margin (179°). Furthermore, the proposed Carlson HHOA/RFPID controller has the maximum bandwidth (fastest response). That means that proposed controller is the most stable system in terms of frequency response criterion.

8 Conclusions

In this research, the influence of approximation techniques on a novel low-order fractionalized proportional–integral–derivative (RFPID) optimal controller for airplane pitch angle control based on the Harris Hawks optimization algorithm (HHOA) is studied. The Carlson, Oustaloup and Matsuda techniques are employed individually to estimate the fractional integral order of the fractionalized PID controller. Based on these comparative studies, we may infer that different approximation methodologies for constructing fractionalized PID controllers result in different sorts of response behavior. The rise time of the system also varies and is highly dependent on the filter and approximation methods used. Transient and frequency responses were applied, and the comparative studies show that the suggested reduced fractional PID based on HHO algorithm with Carlson controller (Carlson HHOA/RFPID) performs better than other controllers in terms of overshoot percentage, settling time, rise time and maximum bandwidth (fastest response).

The aircraft pitch angle control system simulation results demonstrated that the technique of approximation adopted can impact the optimal performance of the optimal adjusting methods. As a result, future research should focus on the role of selected approximation models in the optimum design of the control process in order to avoid degradations in command performance while performing optimal fractional or fractionalized order controllers in applications.

Funding The authors have not received any funding for this research.

Declarations

Conflict of interest The authors affirm no conflicts of interest regarding authorship and research of this article.

References

1. Vinagre BM, Chen YQ, Petráš I (2003) Two direct Tustin discretization methods for fractional-order differentiator/integrator. J. Frankl. Inst. 340:349–362
2. Idir A, Kidouche M, Bensafia Y, Khettab K, Tadjer SA (2018) Speed control of DC motor using PID and FOPID controllers based on differential evolution and PSO. Int. J. Intell. Eng. Syst. 11:241–249
3. Idir A, Canale L, Tadjer SA, Chekired F (2022) High order approximation of fractional PID controller based on grey wolf optimization for DC motor. In: 2022 IEEE international conference on environment and electrical engineering and 2022 IEEE industrial and commercial power systems Europe (EEEIC/I&CPS Europe), Jun 2022, Prague, Czech Republic. pp 1–6
4. Idir A, Akroum H, Tadjer SA, Canale L (2023). A comparative study of integer order PID, fractionalized order PID and fractional order PID controllers on a class of stable system. In: 2023 IEEE international conference on environment and electrical engineering and 2023 IEEE industrial and commercial power systems Europe (EEEIC/I&CPS Europe), pp 1–6. IEEE
5. Idir A, Bensafia Y, Khettab K, Canale L (2022) Performance improvement of aircraft pitch angle control using a new reduced order fractionalized PID controller. Asian J Control 25:2588–2603
6. Podlubny I, Dorcak L, Kostial I (1997) On fractional derivatives, fractional-order dynamic systems and PI/sup/spl lambda//D/sup/spl mu//-controllers. In: Proceedings of the 36th IEEE conference on decision and control, vol 5, pp 4985–4990. IEEE
7. Luo Y, Chen YQ, Wang CY, Pi YG (2010) Tuning fractional order proportional integral controllers for fractional order systems. J Process Control 20(7):823–831
8. Bensafia Y, Khettab K, Idir A (2018) An improved robust fractionalized PID controller for a class of fractional-order systems with measurement noise. Int J Intell Eng Syst 11(2):200–207
9. Idir A, Khettab K, Bensafia Y (2022) Design of an optimally tuned fractionalized PID controller for dc motor speed control via a henry gas solubility optimization algorithm. Int J Intell Eng Syst 15(2)
10. Soukkou A, Leulmi S (2016) Controlling and synchronizing of fractional-order chaotic systems via simple and optimal fractional-order feedback controller. Int J Intell Syst Appl 8(6):56
11. Vinagre BM, Podlubny I, Hernandez A, Feliu V (2000) Some approximations of fractional order operators used in control theory and applications. Fract Calc Appl Anal 3(3):231–248
12. Khovanskii AN (1963) In: Peter Wynn P, Noordhoff NV (eds) The application of continued fractions and their generalizations to problems in approximation theory, Translated by Alexey Nikolaevitch Khovanskii: 28 (p 212). Groningen: Dfl. Translated by1963
13. Deniz FN, Alagoz BB, Tan N, Atherton DP (2016) An integer order approximation method based on stability boundary locus for fractional order derivative/integrator operators. ISA Trans 62:154–163
14. Wei Y, Wang J, Liu T, Wang Y (2019) Fixed pole based modeling and simulation schemes for fractional order systems. ISA Trans 84:43–54
15. Bingi K, Ibrahim R, Karsiti MN, Hassan SM, Harindsan VR (2020) Approximation techniques. In: Fractional-order systems and PID controllers. Studies in systems, decision and control. Springer, Cham, p 255
16. Izci D, Ekinci S, Demirören A, Hedley J (2020) HHO algorithm based PID controller design for aircraft pitch angle control system. In: 2020 international congress on human-computer interaction, optimization and robotic applications (HORA), pp 1–6. IEEE
17. Carlson G, Halijak C (1964) Approximation of fractional capacitors (1/s)^(1/n) by a regular Newton process. IEEE Trans Circuit Theory 11(2):210–213
18. Matsuda K, Fujii H (1993) H (infinity) optimized wave-absorbing control-Analytical and experimental results. J Guid Control Dyn 16(6):1146–1153
19. Charef A, Sun HH, Tsao YY, Onaral B (1992) Fractal system as represented by singularity function. IEEE Trans Autom Control 37(9):1465–1470
20. Oustaloup A, Levron F, Mathieu B, Nanot FM (2000) Frequency-band complex noninteger differentiator: characterization and synthesis. IEEE Trans Circuits Syst I Fundam Theory Appl 47(1):25–39

21. Xue D, Zhao C, Chen Y (2006) A modified approximation method of fractional order system. In: 2006 international conference on mechatronics and automation, pp 1043–1048. IEEE
22. "Control Tutorials for MATLAB and Simulink - Aircraft Pitch: System Modeling," Published with MATLAB® 7.14, 2012. http://ctms.engin.umich.edu/CTMS/index.php?example=AircraftPitch&section=SystemModeling (accessed Jul. 5, 2022)
23. Tepljakov A, Petlenkov E, Belikov J (2011) FOMCOM: a MATLAB toolbox for fractional-order system identification and control. Int J Microelectron Comput Sci 2(2):51–62
24. Chen Y, Petras I, Xue D (2009) Fractional order control-a tutorial. In: 2009 American control conference, pp 1397–1411. IEEE
25. Idir A, Canale L, Bensafia Y, Khettab K (2022) Design and robust performance analysis of low-order approximation of fractional PID controller based on an IABC algorithm for an automatic voltage regulator system. Energies 15(23):8973
26. Caputo MC, Torres DF (2015) Duality for the left and right fractional derivatives. Signal Process 107:265–271
27. Ortigueira MD (2011) Fractional calculus for scientists and engineers, vol 84. Springer Science & Business Media, Berlin
28. Kaçti V, Ekinci S, Davut İZCİ (2020) Efficient controller design for aircraft pitch control system using henry gas solubility optimization. Dicle Üniversitesi Mühendislik Fakültesi Mühendislik Dergisi 11(3):953–964
29. Kilbas AA, Srivastava HM, Trujillo JJ (2006) Theory and applications of fractional differential equations, vol 204. Elsevier, Amsterdam
30. Bensafia Y, Khettab K, Idir A (2022) A novel fractionalized PID controller using the sub-optimal approximation of FOTF. Algerian Journal of Signals and Systems 7(1):21–26
31. Shrivastava N, Varshney P (2018) Implementation of Carlson based fractional differentiators in control of fractional order plants. Int J Intell Syst Appl 11(9):66
32. Xue D, Chen Y (2005) Sub-optimum H2 rational approximations to fractional order linear systems. In: International design engineering technical conferences and computers and information in engineering conference, vol 47438, pp 1527–1536